

Thermoelectrics

Unveiling Crucial Chemical Processing Parameters Influencing the Performance of Solution-Processed Inorganic Thermoelectric Materials

Christine Fiedler, Mariano Calcabrini, Yu Liu, and Maria Ibáñez*

Abstract: Production of thermoelectric materials from solution-processed particles involves the synthesis of particles, their purification and densification into pelletized material. Chemical changes that occur during each one of these steps render them performance determining. Particularly the purification steps, bypassed in conventional solid-state synthesis, are the cause for large discrepancies among similar solution-processed materials. In present work, the investigation focuses on a water-based surfactant free solution synthesis of SnSe, a highly relevant thermoelectric material. We show and rationalize that the number of leaching steps, purification solvent, annealing, and annealing atmosphere have significant influence on the Sn:Se ratio and impurity content in the powder. Such compositional changes that are undetectable by conventional characterization techniques lead to distinct consolidated materials with different types and concentration of defects. Additionally, the profound effect on their transport properties is demonstrated. We emphasize that understanding the chemistry and identifying key chemical species and their role throughout the process is paramount for optimizing material performance. Furthermore, we aim to demonstrate the necessity of comprehensive reporting of these steps as a standard practice to ensure material reproducibility.

1. Introduction

Thermoelectric (TE) devices directly and reversibly convert heat into electricity, offering unique possibilities for energy harvesting and thermal management.^[1] The efficiency of TE devices is primarily determined by the properties of the materials used. Materials with enhanced performance combine a high electrical conductivity (σ), high Seebeck coefficient (S) and low thermal conductivity (κ).^[2] To date, the materials that display a better balance between these properties are dense inorganic semiconductors. Polycrystalline semiconductors are desired, because of their superior mechanical strength and lower fabrication costs compared to their single-crystal counterparts.^[3]

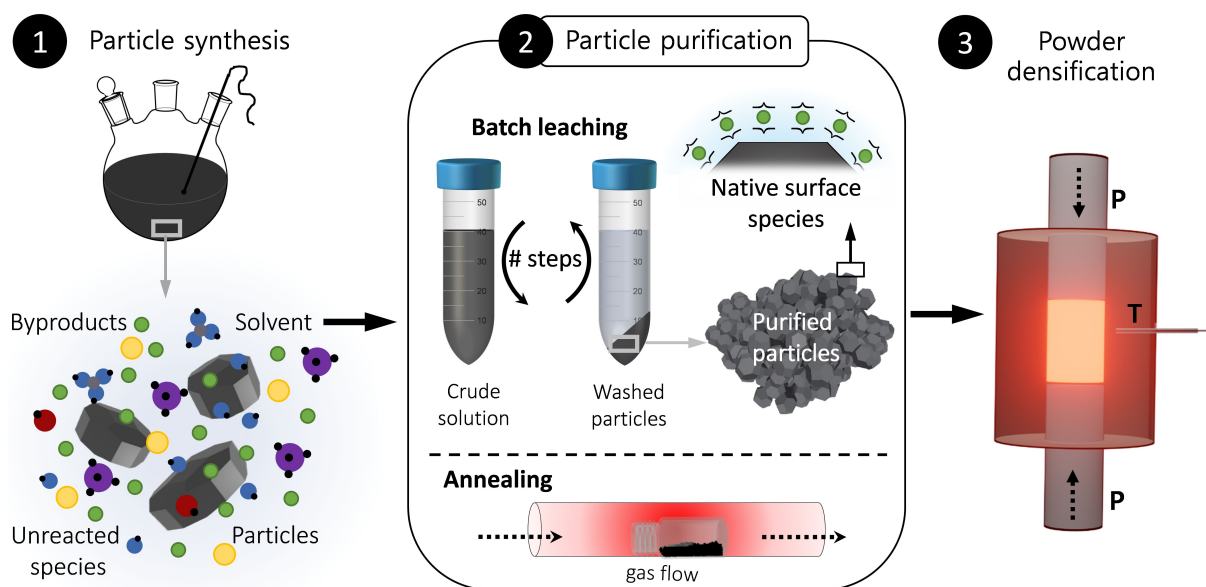
Typically, the fabrication of polycrystalline TE semiconductors involves a two-step process: initially preparing the semiconductor in powdered form, followed by consolidating the powder into a dense material.^[4] The powder is most commonly prepared through high temperature reactions or mechanical alloying; these processes are energy intensive and achieving precise control over particle size and size distribution of the powder is challenging.^[4] In recent years, solution-processing (hydrothermal, solvothermal and aqueous)^[5–9] has gained considerable attention as a possible cost-effective and scalable way of producing high-performance TE materials. Compared to the traditional approaches, milder conditions are used, including lower reagent purity, reduced temperatures and shorter reaction times.^[9–11] A further advantage of solution-processing is that it provides avenues to produce particles with finely controlled characteristics, e.g., size, shape, composition and crystal phase, that can translate into determining properties and characteristics of the final material.^[1,10,12,13]

Despite the numerous advantages of solution-processing, an overall complexity arises from the multiple processes involved: 1) particle synthesis, 2) particle purification, and 3) powder densification (Scheme 1).^[14] The multiple processes provide many opportunities for material control and optimization, which is contingent upon understanding the underlying phenomena that takes place in each one of the processing steps. To date, there has been limited work explaining the effects of each of the processing steps on the final material. Most reports have focused on developing new synthetic strategies for the particles, implementing novel surface treatments^[15–17] or exploring thermal treatments^[18–20] to achieve high performance. However, one of the most

[*] C. Fiedler, Dr. M. Calcabrini, Dr. Y. Liu, Prof. M. Ibáñez
Institute of Science and Technology Austria,
Am Campus 1, 3400 Klosterneuburg, Austria
E-mail: mibanez@ista.ac.at

Dr. Y. Liu
School of Chemistry and Chemical Engineering
Hefei University of Technology,
230009, Hefei, China

© 2024 The Authors. Angewandte Chemie International Edition published by Wiley-VCH GmbH. This is an open access article under the terms of the Creative Commons Attribution Non-Commercial NoDerivs License, which permits use and distribution in any medium, provided the original work is properly cited, the use is non-commercial and no modifications or adaptations are made.



Scheme 1. Steps involved in the solution-processing of TE materials.

crucial processes has been completely neglected: the purification process.

Powders produced in solution require a series of purification steps, to separate the particles from the solvent, unreacted species, and soluble byproducts. Variations in purification methods and conditions such as solvent used and its quantity, number of purification cycles, and duration can result in different types and concentration of impurities, which consequently, influences the composition, microstructure, and transport properties of the final material. Despite the importance of the purification step of solution-processed materials, it is always just used as a means to an end. As a result, two interconnected problems arise. On the one hand, since the importance of purification is underrated, there is a lack of thorough reporting on how the purification is conducted, i.e. volumes used, choice of solvent or even the number of times the particles are purified.^[11,19,21–25] This causes problems with reproducibility. On the other hand, disregarding the chemistry that occurs during the purification process hampers performance optimization, and even impedes the development of novel materials.

In this work, we study the chemistry of the purification process; specifically, we unveil the impurities and byproducts that remain after the synthesis of the powder by taking a closer look at the synthesis. We center our investigation on SnSe, one of the highest performing TE materials to date,^[26] and investigate the effect of the purification solvents and the number of leaching steps on the impurities present in the densified material and correlate these processing parameters to the transport properties of the final TE semiconductor. While this work focuses on bare SnSe, most of the phenomena described here can be extrapolated to other materials, especially those produced using polar solvents without surfactants. Moreover, this knowledge enables the rational performance optimization of the final polycrystalline material through developing efficient purification proc-

esses and establishes the need for reporting material preparation precisely so that outstanding results can be reproduced. Such an understanding is not limited only to TEs but is also applicable to other fields that use solution-processed particles and/or semiconductors such as photovoltaics, sensors, batteries and catalysis.^[27]

2. Results and Discussion

Solution-based syntheses surged as a viable alternative to prepare TE materials from particles made in solution.^[10,11,19,28–31] Particle syntheses can be performed with or without surfactants (also called ligands), at temperatures ranging from room temperature to around 350 °C, with reaction times spanning from a few minutes^[32,33] to even hours.^[8,15,34] Solvents employed range from water^[7,8,35,36] to organic solvents^[37] and molten salts,^[38] in some cases under pressure, e.g. solvothermal.^[5,35] For this work, we use a surfactant-free aqueous synthesis as it is cheaper than any other reported method and suitable for scaling to industrial levels. The synthesis uses neither organic solvents nor surfactants, has a short reaction time (2 h) and is conducted at low temperature (ca. 100 °C). The water-based synthesis is also very versatile, allowing for modifications such as doping, to further tailor the TE performance.^[31,39,40] Additionally, this synthetic approach has demonstrated to yield various TE materials with enhanced performance, e.g. PbS,^[7] Bi₂Te₃,^[40] Ag₂Se^[8] and SnSe.^[8,15,41] Despite its importance and extended use on different systems, detailed studies in many of the reported systems is missing.

For this work, we selected SnSe, as it is of significant importance in TEs, owing to its exceptional performance.^[15,26,42] In addition, modifications of the particles obtained through the used synthetic method has yielded one of the most outstanding performances achieved

through solution aqueous synthesis to date.^[15] In a previous study, we showed that for the solution-synthesis of electrostatically stabilized SnSe colloids, the presence of surface adsorbates is unavoidable, and demonstrated their influence on the TE properties.^[43] Here, we address the need for a deeper understanding of the system and the chemistry in detail of the synthesis and purification process to understand the resulting transport properties of the consolidated materials.

2.1. Particle Synthesis

The synthesis uses Se powder and $\text{SnCl}_2 \cdot 2\text{H}_2\text{O}$ as the precursors.^[15,31,43] A comprehensive explanation of the chemistry of this synthesis requires balanced chemical equations and thermodynamic constants that describe the multiple equilibria. The accurate description of the chemical species present is complex, and far from the scope of this work. However, due to the importance in identifying the species present in the final crude solution, we provided a comprehensive description of the chemical reactions occurring throughout the processes in the Supporting Information (SI) as well as pH-dependent speciation diagrams, and charge and mass balances (Figure S1–S3, Section A). All thermodynamic data was calculated using literature values and can also be found in the Supporting Information (Table S1–S2). For simplification, we refer almost exclusively to the most concentrated species in solution (Figure 1).

2.2. Purification of the Powder

The aim of any purification is to remove impurities, unreacted species, and byproducts of the reaction. In the lab-scale, the purification of large particles can be done by dialysis,^[44] filtration,^[45] size chromatography,^[46] or leaching.^[47] Among them, batch leaching (referred to commonly as precipitation/redispersion) is the most common impurity-extraction technique for the aqueous synthesis highlighted in this work due to its simplicity and ease of scalability. In batch leaching, impurities are dissolved in a liquid phase, which is subsequently separated from the particles by centrifugation or decantation. The extraction of impurities depends on three factors: i) the solubility of impurities in the liquid phase, ii) the adsorption of the impurities on the particle surface and iii) the amount of liquid (used in the leaching process) trapped within the particles that cannot be separated.

In our system, based on the reactions described in the previous section, the as-synthesized SnSe particles are suspended in a solution that contains Na^+ , Cl^- , $\text{B}(\text{OH})_4^-$, OH^- , and $\text{Se}^{2-}/\text{HSe}^-$ (ca. 10% excess, Figure S4) (Figure 1). Intuitively, polar solvents are the best choice for dissolving these impurities. Common polar solvents used include water, ethanol, acetone, isopropanol and methanol.^[48] When selecting an ideal solvent there are several factors to take into account including, its capacity to dissolve the impurities, compatibility with the chosen purification technique, volatility, safety, cost, and environmental impact. The purification process done as reported in our previous works includes

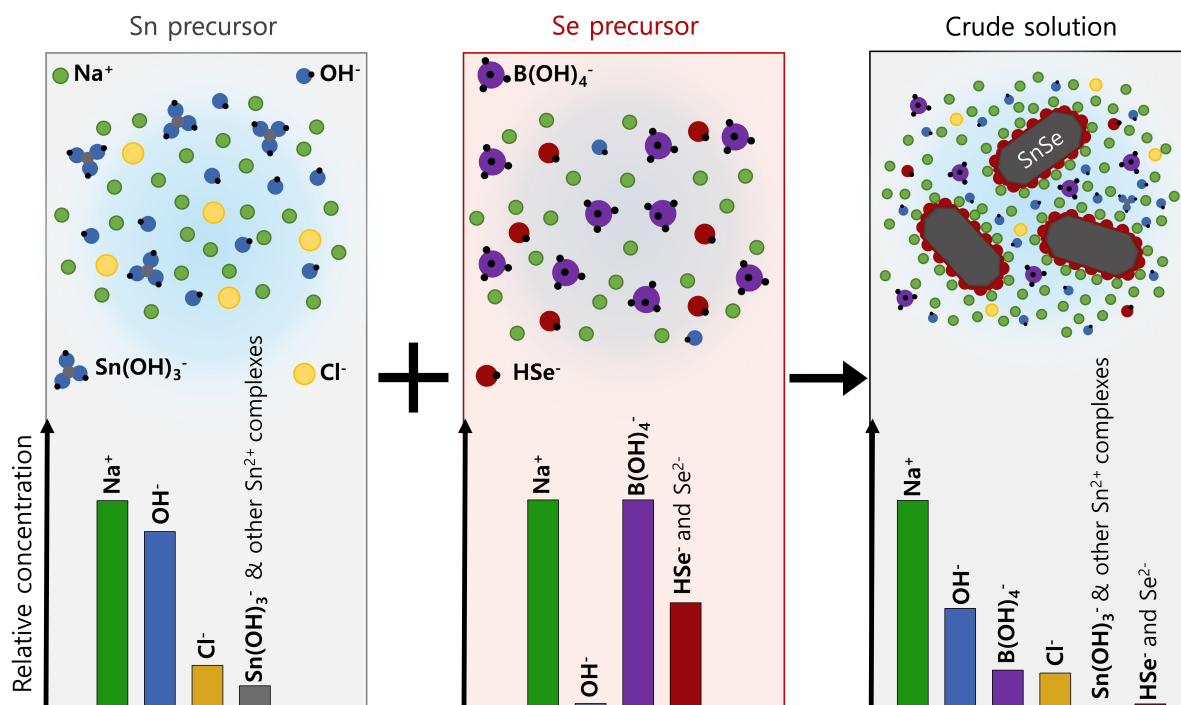


Figure 1. Reaction Scheme illustrating the ions present in each precursor and the resultant suspension of SnSe particles after mixing, along with the reaction byproducts and unreacted ionic species. The bar plots qualitatively show the concentration of the different species in solution relative to the most concentrated ion, Na^+ .

6 precipitation/re-dispersion steps alternating water and ethanol as leaching solvents followed by annealing under a reductive atmosphere (5% H₂ in N₂, 500 °C, 1 h). For this study, details on the leaching process including vortex-mixing times, sonication times, solvent volumes and centrifugation speeds can be found in the Supporting Information (section: Purification of the SnSe particles). After this purification process, the particles in solution are negatively charged (zeta potential = -23 ± 5 mV) with significant amounts of Na⁺ ions electrostatically adsorbed on the particle surface preserving charge neutrality.^[43,49] As Na⁺ does not form volatile species or decompose at the processing temperatures; it remains in the material after the annealing and sintering processes. In the final material, the content of Na is beyond its solubility limit in SnSe (<1% at.),^[49] resulting in its segregation. Consequently, Na not only distributes within the lattice as a dopant, but also as Na-rich nanoprecipitates, dislocations and grain boundary complexions. Overall, the presence of Na in the final material translates in: i) higher carrier concentrations as Na⁺ occupies Sn²⁺ lattice sites acting as a *p*-type dopant, ii) lower hole mobilities at room temperature, iii) a relatively high *S*, caused by energy barriers at the interface between Na-rich segregates and SnSe grains, and iv) lower κ due to phonon scattering at different length scales.^[15,43] Figure 2 represents a summary of the standard material processing, and the corresponding structural characteristics and their effects on the transport properties.

In the following sections, the material obtained using the described leaching process ($\times 6$ leaching steps) serves as the reference for comparison with the outcome attained with different parameters, as is the processing that results in the highest thermoelectric performance. All other processing parameters will remain constant, i.e. all samples were annealed at 500 °C for 1 h under forming gas (5% H₂ in N₂) and densified by spark plasma sintering (SPS) at 47 MPa, 500 °C for 5 min. Samples were measured in the direction

parallel to the pressing axis as it shows the highest TE performance with a zT_{\max} of 1.32 (Figure S5). All sample densities (>91%) can be found in the Supporting Information (Table S3–S8) together with details of the temperature and pressure profiles applied to form the pellets (Pellet consolidation).

The transport properties of the samples prepared with this standard purification method (represented in black squares in all graphics) are used to compare the effects of different purification conditions. Therefore, the transport properties are explained based on the microstructure and changes in the material composition.

2.2.1. Choice of Purification Solvent

In a synthesis conducted in polar media, particularly for water-based systems, water is the first choice to remove impurities, since it combines low cost, a low carbon footprint, and a very high dissolution power for ionic species. Water is often used in combination with other solvents, especially ethanol and isopropanol.^[36] The reason is mainly because low boiling point alcohols evaporate quickly helping to achieve drier powders and remove traces of water as they are miscible. Alcohols also have low toxicity, allow small colloids to precipitate more easily than water due to their lower dielectric constant, and are environmental-friendly.^[21] Based on the standard leaching process we delve into what impurities the used solvents are actually removing and examine the supernatants from each leaching step.

In the first step, the solution containing Na⁺, OH⁻, Cl⁻, B(OH)₄⁻, and Se²⁻ (SI, Section B) is separated from the particles by centrifugation without any addition of solvent (step 0: crude mixture). After the precipitation of SnSe particles, the supernatant containing all those ionic species is discarded. The precipitated powder is then re-dispersed in fresh water through vortex mixing and sonication (step 1:

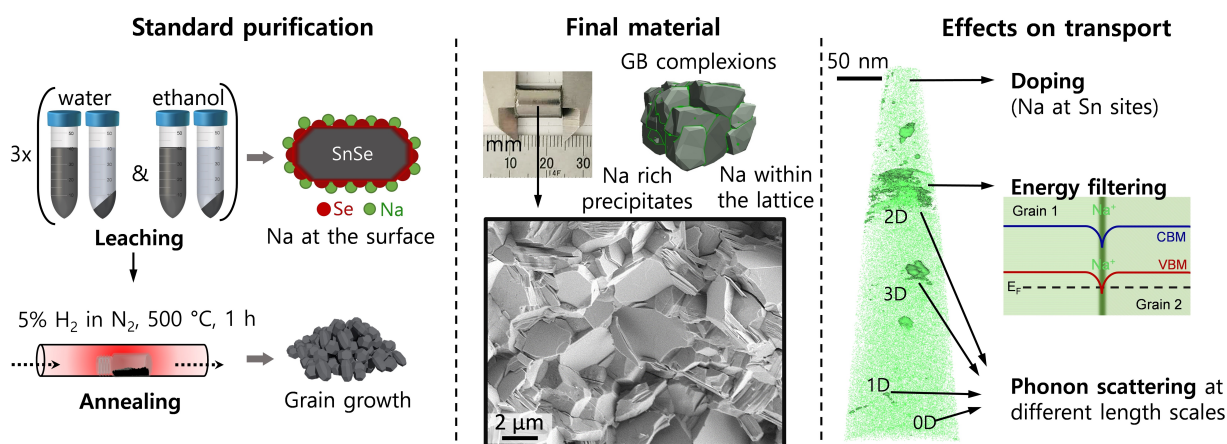


Figure 2. Overview of the material purification and the influence Na⁺ has on the development of the final materials' structure and transport properties. Adsorbed Na⁺ on the particles is unavoidable, resulting in enhanced coarsening of the particles during the annealing process. In the densified material, some Na remains within the lattice, and segregates to dislocations, precipitates and to the grain boundaries, leading to the formation of complexions and precipitates. These defects alter completely the transport properties.^[43]

H₂O-1). The new mixture is then centrifuged, and the resulting supernatant analyzed. Due to the adsorption of cations on the particles and the liquid trapped within the particles, which has a high concentration of ionic species (same as in the crude mixture), the new supernatant still contains impurities. The concentration of these ions in the new supernatant significantly decreases with respect to the crude mixture, except for the concentration of Sn²⁺ complexes (Figure 3a, analyzed with ¹¹⁹Sn and ¹¹B NMR, Figure S6). This is caused by the dissolution of Sn²⁺ from the surface of the particles facilitated by the basic pH (ca. 13) and the removal of free Se²⁻ in the previous step (Equation S1b). The aqueous supernatant is discarded, the precipitated particles re-dispersed in ethanol and the leaching procedure is repeated (step 2: EtOH-2). The ethanolic supernatant at this point has an intense yellow color which turns red on continuous exposure to air. This coloration indicates a high content of Se species, suggesting that the removal of Se by ethanol is enhanced compared to water (Figure S7). To prove this, we analyzed the UV/Vis absorption spectra of the aqueous and ethanol supernatants (Figure 3b). We identified three different Se species: Se₂²⁻, Se₃²⁻ and Se₄²⁻ in the ethanol supernatants. These experiments indicate that water is more efficient in removing Sn, while ethanol is more efficient in removing Se.

The process continues alternating between water (step 3: H₂O-3 and step 5: H₂O-5) and ethanol (step 4: EtOH-4 and step 6: EtOH-6), where the continuous leaching of Sn with water and Se with ethanol decreases in magnitude with every leaching step as the pH approaches neutrality (Figure 3a) and an equilibrium composition is approached.

The effects observed during the leaching procedure are further confirmed by leaching the particles exclusively with water or ethanol, keeping the same total number of purification steps. For all samples washed with water, ethanol, and water/ethanol, neither scanning electron microscopy (SEM) nor X-ray diffraction spectroscopy (XRD) revealed obvious differences in the microstructure (Figure S8); therefore, we attribute any differences to changes in the composition of the samples that occur due to the partial dissolution in the leaching solvents. It should be noted that precise quantitative elemental analysis of SnSe poses difficulties, primarily due to challenges associated with the presence of Sn oxide impurities. After the final leaching step, and irrespective of the solvent used, the particles still have an excess of Na⁺ as it is electrostatically adsorbed and cannot be completely removed.

The differences in the transport properties between the materials produced by leaching with different solvents can be attributed to the resulting Sn:Se ratio and the presence of SnO or SnO₂ as trace secondary phases.^[50] We consider these are not visible as most probably there are below the XRD detection limit. When water is used, either alone or in combination, the removal of Sn results in an increase of ionized Sn vacancies (V''_{Sn})^[51,52] leading to higher carrier concentrations ($p_{H,water}$: $1.5 \times 10^{19} \text{ cm}^{-3}$, $p_{H,water/ethanol}$: $2.2 \times 10^{19} \text{ cm}^{-3}$, Table S4) than when ethanol is the only leaching solvent ($p_{H,ethanol}$: $0.7 \times 10^{19} \text{ cm}^{-3}$). This leads to a higher σ and lower S (Figure 3c and d respectively) compared to samples washed with just ethanol. Moreover, we attribute the difference between only water and water/ethanol combination to the synergistic effect in removing Sn from the surface when both solvents are used shifting even

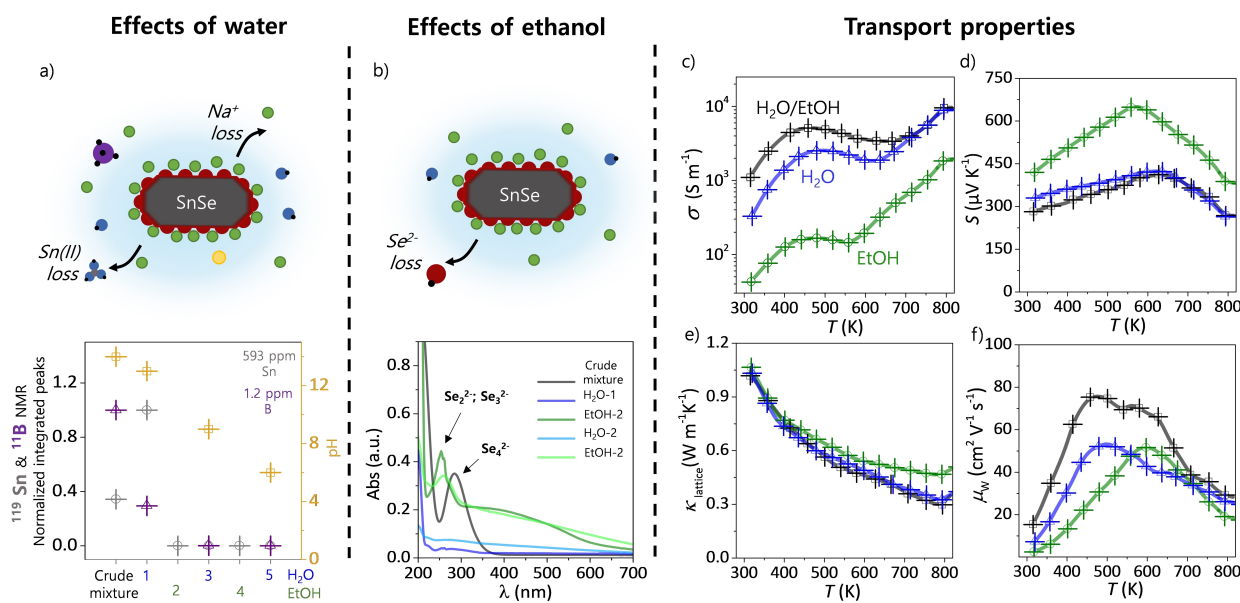


Figure 3. Effect of the purification solvents on the transport properties of SnSe. a) Effect of leaching with water on the composition of the particles and the removal of Sn and B(OH)₄⁻ in aqueous and ethanol supernatants determined by ¹¹⁹Sn (grey points) and ¹¹B NMR (purple points) respectively. b) Effect of ethanol on the removal of Se from the samples and UV/Vis absorption spectra of aqueous and ethanol supernatants showing that ethanol continues to remove Se_n²⁻ after multiple leaching steps while water does not. c) electrical conductivity, d) Seebeck coefficient, e) lattice thermal conductivity and f) weighted mobility of samples prepared by leaching with water, ethanol, and alternating water and ethanol.

further the off-stoichiometry of SnSe toward more Se rich for the materials produced by washing with the 2 solvents. When the particles are washed with only ethanol, the removal of Se shifts the material composition in the opposite direction, reducing the content of Sn vacancies and resulting in a material with less holes.

Another big difference between the samples washed with ethanol and water is the carrier mobility. Overall, when only ethanol is used, the carrier mobility is the lowest: $\mu_{H,Ethanol}$ $0.3 \text{ cm}^2 \text{ V}^{-1} \text{ S}^{-1}$. We ascribed this to: i) the lower efficiency of ethanol in removing ionic impurities since ethanol is less polar than water, and ii) the shift in composition that may lead to the formation of different trace secondary phases based on the thermodynamics of oxide formation in the Sn–Se–O system.^[50] Both phenomena lead to the formation of carrier scattering lowering the carrier mobility. The lower mobility in the case of using only water ($\mu_{H,water}$ $0.9 \text{ cm}^2 \text{ V}^{-1} \text{ S}^{-1}$) compared to the combination of solvents ($\mu_{H,water/ethanol}$ $2.3 \text{ cm}^2 \text{ V}^{-1} \text{ S}^{-1}$) can be attributed to the same phenomena described for the carrier concentration. We suggest that, the reason behind the increase in mobility is because water removes Sn from the surface, and then the intermediate ethanol washings remove Se, facilitating further removal of Sn and other impurities by the later water washings. In turn, this leads to cleaner grain interfaces and to a higher carrier mobility.

Regarding the thermal conductivity, we present here the lattice thermal conductivity ($\kappa_{lattice}$) to remove any possible dependence on the different effects of charge carriers. Clearly, the difference in composition and microstructure induced by washing with different solvents that have such dramatic effects on the electrical properties have very little effect on the thermal conductivity. This is in line with the recent work regarding the effect of composition and oxide secondary phases in the thermal transport of polycrystalline SnSe.^[50] Overall the $\kappa_{lattice}$ remains low, of which we attribute to the strong lattice anharmonicity in SnSe.^[43,53] Similarly, the only difference we observe is in the material purified only with ethanol that increases at high temperatures. This difference could be attributed to the effect of secondary phases when the material is shifting towards a more Sn-rich composition as mentioned in the work by Isotta et al.^[50] A change on the order of the solvents used during the leaching steps, starting with ethanol instead of water, has minimal effects on the material performance (Figure S9).

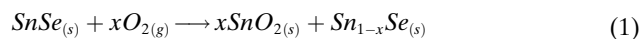
2.2.2. Number of Precipitation/Re-Dispersion Steps

Conducting multiple precipitation/ redispersion steps for the purification of particles is crucial to ensure the removal of impurities. We observed that, while some studies use three leaching steps for this exact synthesis,^[21] others opt for six,^[15,43] and many more do not report how many steps are performed.^[11,19,22–25] In this section, we demonstrate the importance of detailing this overlooked process. In the previous section, we explained that alternating water and ethanol as solvents for the leaching process results in materials with higher performance than using only either

solvent. In those experiments, we performed 6 precipitation/ redispersion steps, alternating water with ethanol. In this section, we explore the influence of the number of leaching steps used to remove impurities from the synthesized powder on the microstructure and its transport properties. We rationalize the content of impurities based on the pH of the aqueous supernatants and charge balances (SI, Section A), and use this to explain the microstructure and composition of the resulting materials, and their transport properties. Given the observed enhancement in performance when both water and ethanol are used, we consistently conduct an even number of leaching steps and evaluate their effect on: 1) composition, 2) presence of secondary phases, 3) grain size and 4) transport properties. We choose the following nomenclature: $\times 2$ (denotes one leaching step with water and one with ethanol = one cycle), $\times 4$ (two cycles), $\times 6$ (three cycles, standard sample) and $\times 10$ (five cycles).

The number of leaching steps in the purification process determines the composition of the final material and the concentration of impurities. As the number of leaching steps increases, impurities as well as surface Sn and Se are removed. We can roughly estimate the removal efficiency of non-adsorbed impurities considering the volume of solvent trapped within the powder after the centrifugation that is not removed with the supernatant and the volume of solvent used for each leaching step. The volume trapped is roughly one-tenth of the volume added, thus free ions will be diluted by a factor of 10 in each leaching step. After n leaching steps, the concentration of free species (not in equilibrium with the solid) decreases by 10^n . Initially, after only 2–4 steps, a significant drop in impurity concentrations is observed. After 6 steps the most highly concentrated ionic species will be, at most, in the μM range. Remaining impurities, like the Na detected, can only be explained due to electrostatic adsorption on the particles' surface.^[43] With each successive leaching step the pH approaches neutrality, and the concentration of impurities and of soluble Sn and Se species decreases, approaching an equilibrium (Figure 4a). The leaching procedure is completed when the pH is neutral, which reflects a balance between the removal of impurities and the retention of the desired components (SI, Section B).

In aqueous synthesis, the presence of oxygen is unavoidable and given the particles' substantial surface-to-volume ratio the formation of oxides is expected.^[14,54] This fact is further aggravated in SnSe, where the formation of oxides (SnO_x) is practically unavoidable independently of the synthetic technique used as indicated by the phase diagram as a function of the partial pressure.^[50] Different synthetic approaches, including solid state ones, may lead to different quantities and crystalline domains for the oxide phases.^[26,42,55] Additionally, in our solution process, SnO_2 can form by the oxidation of Sn^{+2} by air during the leaching steps and remains in the material throughout the leaching process. Such an oxidation creates Sn vacancies in the material (Equation 1), as well as SnSe_2 (Equation 2).



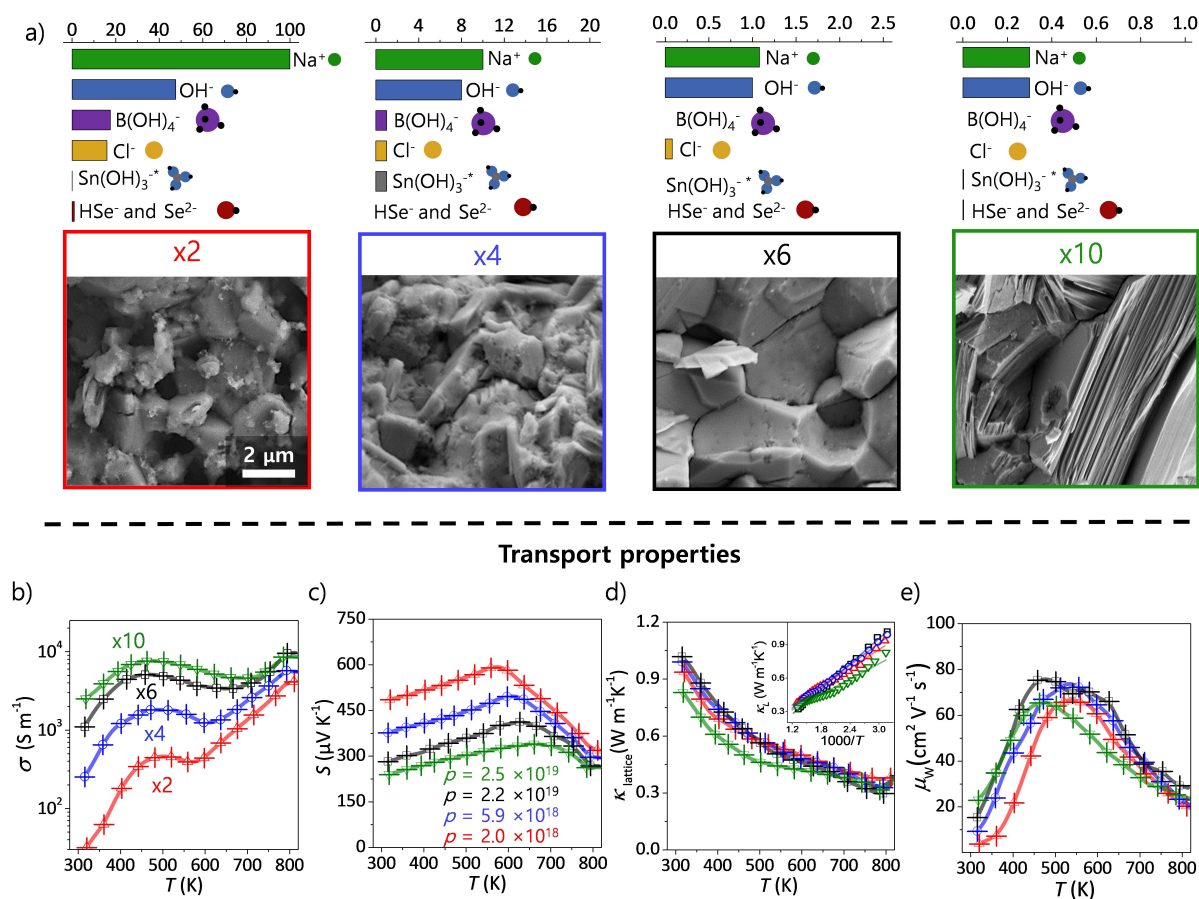
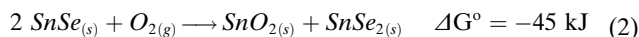


Figure 4. Effect of the number of leaching steps on the structural and functional properties of SnSe. a) SEM of pellets prepared leaching the starting particles $\times 2$, $\times 4$, $\times 6$ and $\times 10$ times, together with a representation of the composition of the removed supernatants estimated from the measured pH and charge and mass balances. b) Electrical conductivity (σ), c) Seebeck coefficient (S), d) lattice thermal conductivity (κ_{lattice}) where the inset shows the plot $1000/T$ -dependent κ_{lattice} and e) weighted mobility (μ_w) of pellets with different number of leaching steps.



If Sn^{2+} is present in a particular supernatant (e.g. H_2O -1, Figure 3a), suggest that the surface of the particles leached in that step, contained a higher content of Sn^{2+} . As the leaching steps are unavoidably conducted in air, SnO_2 will form (Equation 2). As more leaching steps are progressively conducted (i.e., $\times 6$ and $\times 10$), the amount of Sn^{2+} present on the surface of the particles decreases hence these pellets show no detectable secondary phases,^[56] as can be seen by XRD patterns and energy dispersive spectroscopy (EDX) (Figure S8). The absence of SnO_2 XRD reflections in the samples washed more than $\times 4$, does not imply that SnO_2 is not present; but rather that the SnO_2 present falls below the detection limit of the XRD. However, a decrease in the detectable content of SnO_2 with each leaching step is observed and is in direct correlation with the removal of Sn during the leaching steps as shown in the previous section. Therefore, to further reduce their content in the final pellet annealing in a reducing atmosphere is required,^[15,42,42,43] discussed in detail in Section 2.3.

The content of impurities, the ratio Sn:Se, and the presence of secondary phases influence grain growth of the

material and other related coarsening phenomena. All of these affect the type and density of defects within the material. SEM images, show significant differences between all the pellets produced with powders obtained after different leaching steps. If $< \times 4$ cycles are done, the final materials, contain secondary phase nanoprecipitates (Figure 4a). EDX showed that the precipitates contain large quantities of Sn and XRD indicates that this secondary phase is SnO_2 (Figure S10). SnO_2 has very limited solubility in the SnSe matrix^[49] and inhibit grain growth by pinning the grain boundaries.^[57] Consequently, pellets obtained from $\times 2$ and $\times 4$ leaching cycles have much smaller grains. With increasing number of leaching steps the grain size increases and ultimately with $\times 10$ leaching steps a degree of texture in the final material is obtained.^[58,59] This is consistent with the removal of the surface Sn^{2+} that leads to smaller amounts of SnO_2 , reducing the pinning effect, and enhancing the growth of the grains (Figure 4a).

With such significant differences in the composition and microstructure very distinct transport properties are expected. As discussed in Section 2.1, the differences in transport properties can be linked to the Sn:Se ratio and the presence of SnO_x . With every successive leaching step, the

removal of Sn results in an increase of Sn vacancies in the consolidated material, leading to higher carrier concentrations (Figure 4c). This leads to a high σ and lower S (Figures 4b and c). This is also coupled with the fact that there is also an increase in the carrier mobility (μ_H) with every leaching step, (μ_H : $\times 2$, $1 \text{ cm}^2 \text{ V}^{-1} \text{ S}^{-1}$; $\times 4$, $2 \text{ cm}^2 \text{ V}^{-1} \text{ S}^{-1}$; $\times 6$, $2.3 \text{ cm}^2 \text{ V}^{-1} \text{ S}^{-1}$ and $\times 10$, $6 \text{ cm}^2 \text{ V}^{-1} \text{ S}^{-1}$) (Figure S11). With the progressive removal of ionic impurities and the decrease in SnO_x , the materials have larger crystalline domains, hence carrier mobility is enhanced due to the decrease in charge scattering. Although there is a decrease in the Seebeck coefficient with increasing number of leaching steps, in all samples the Seebeck coefficient is still higher than the calculated Pisarenko relation (Figure S12). This phenomenon is attributed to energy filtering^[15,43] and is still prevalent in all samples.

Even though the significant differences in composition and microstructure result in variations in the σ and S , minor effects are observed for the κ_{lattice} . As discussed previously, this is also in accordance with the effect of oxides as secondary phases and composition influence in polycrystalline SnSe.^[50] The inset of Figure 4d shows the curves of κ_{lattice} versus $1000/T$ for every purification cycle, from which all κ_{lattice} values show a roughly linear relationship, which is an indication that Umklapp phonon scattering plays the most significant role in SnSe. Despite $\times 10$ leaching steps leads to bigger grains and a higher conductivity, the sample with $\times 6$ leaching steps has an optimal power factor (PF : σS^2) due to the tradeoff between the electrical conductivity and the Seebeck coefficient. It should be noted that strict adherence to the protocol ensures consistency and reproducible results for all samples (Figure S13).

2.2.3. Removing Volatile Impurities by Annealing

Leaching and drying is generally not enough to achieve completely purified powders, especially as complete removal of the solvent is not straightforward, and there could be labile and volatile impurities that couldn't be removed by the leaching steps. Moreover, depending on the material in question and the size of the particles, even secondary phases can be present or appear during the pressure assisted sintering process. In order to control the outcome of the sintering process and render materials that are stable during the temperature dependent transport measurements, annealing the powders prior to powder densification is imperative.

Surprisingly, this annealing step is not always performed. In the case of surfactant-stabilized particles, it is commonly done to remove the insulating organic surfactants by thermally decomposing them.^[60–62] Differently, in surfactant-free solution-processed syntheses, the particle's surface is most often considered naked and annealing is rarely performed,^[40,63] except for cases where a specific chemical reaction is sought, such as reduction of oxide species,^[42] or to convert capping molecules into crystalline nanoparticles.^[64,65]

In this section, we demonstrate how an annealing step before SPS is necessary to ensure sample stability. We

achieve this by comparing 3 samples prepared almost identically, with the only difference being the annealing step prior to sintering. In the first case the powder is directly sintered (no annealing). In the second and third cases, an annealing step is conducted under a flow of inert gas (N_2 , 500°C , 1 h) and in forming gas (5 % H_2 in N_2 , 500°C , 1 h) before sintering, respectively. All the other processing parameters are done the same way as the standard sample.

Annealing induces changes in the structure and the composition of the powder. During the annealing, the particles increase in grain size, from 150 nm to 680 nm (Figure S14), promoted by the presence of low melting point Na_2Se_n on the outside of the grains.^[43,66–68] Furthermore, these polyselenides (Na_2Se_n) partially decompose during the annealing, eliminating some of the excess Se ($T_{\text{m, se}}$: 220.8°C) of the Se-terminated particles. Besides, any traces of adsorbed solvent (water and ethanol) are also removed (Figure 5a). This was also observed for samples annealed in N_2 (Figure S15), where three heating and cooling cycles were conducted with no degradation of the material.

When the annealing step is avoided, the powder (ca. 150 nm) yields pellets with consistently smaller grains (Figure 5d), despite the temperature of the sintering process is the same as the annealing step. However, non-annealed powder produce pellets that are not stable, which under multiple cycles of measurements develop pores, microcracks, and swell. We correlate this to the removal over time of volatile impurities (excess Se, adsorbed solvent), that leads to significant microstructural changes. Such structural changes consequently affect the transport properties. While the initial σ of both samples is similar (Figures 5e and f), the sample prepared without annealing degrade continuously with every heating and cooling measurement cycle. In subsequent measurement cycles, the σ of the non-annealed samples decreases due to the structural damage of the pellet. A similar behavior is observed for the S , which increases as the structural changes render the material more insulating.

Annealing can be also used to tune the material's composition.^[69–73] For instance, non-volatile, non-labile impurities that remain after leaching can also be removed if they react with the annealing gas yielding volatile products. This is the case of oxides, which can be almost unavoidable in certain semiconductors, as the case of SnSe.^[50] The way to remove oxide impurities is chemical reduction. In some cases, measures can be taken to prevent air exposure and oxidation of the particles, but certain materials are extremely prone to oxidation; moreover, when the synthesis and particle leaching are conducted in water, oxidation is practically unavoidable.^[74,75] Lee et al. proposed annealing in a reducing atmosphere (3–5 % H_2 in an inert carrier gas) for a long period of time to remove surface oxides from SnSe.^[42] Annealing with H_2 can reduce SnO_2 to SnO (Equation 3) but long reaction times and high temperatures are required to drive the reaction. The oxidation of Sn also results in the formation SnSe_2 as a secondary phase, therefore when SnO is reduced, results in the conversion back to SnSe (Equation 4).

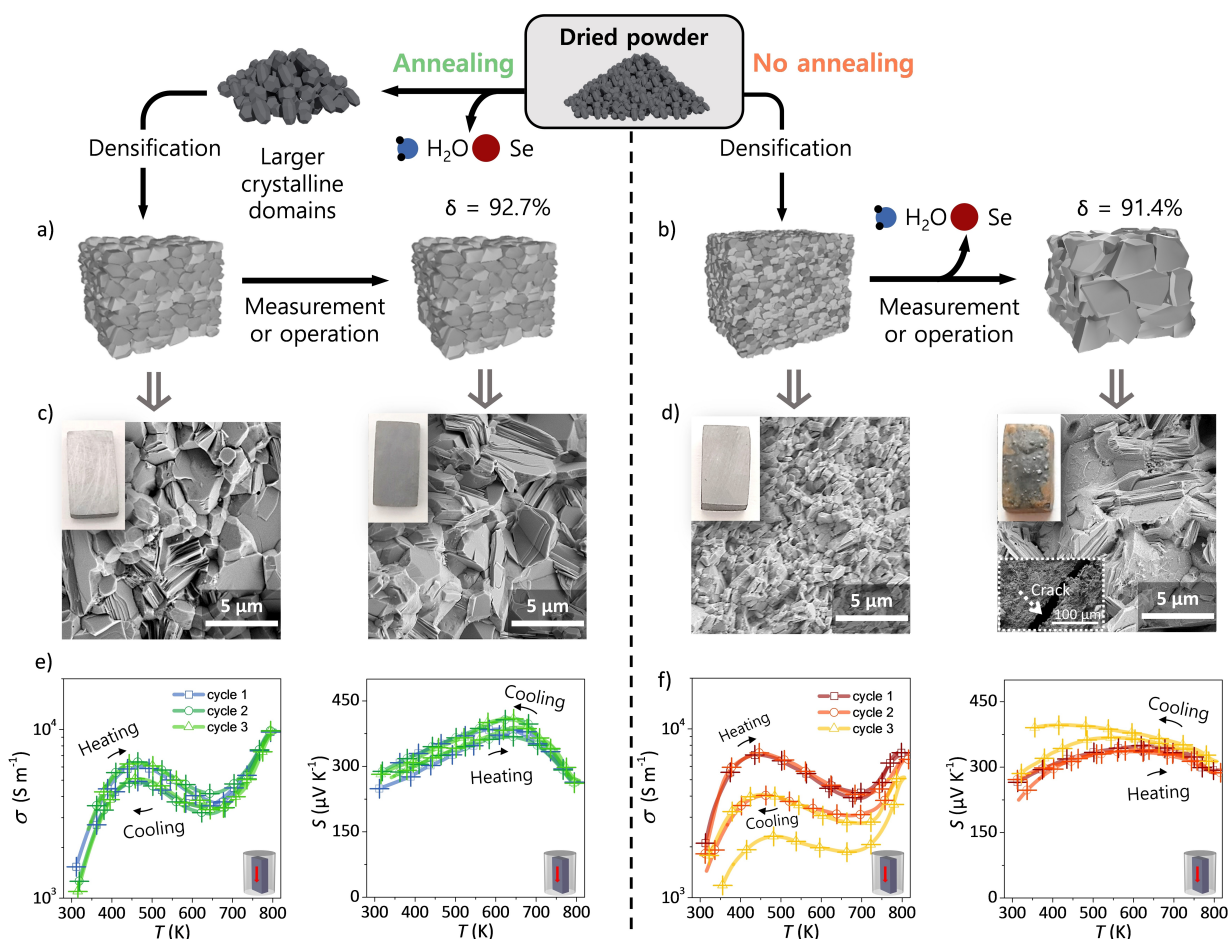
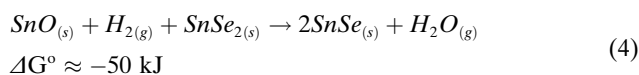


Figure 5. Structural and functional properties of SnSe pellets prepared with and without annealing. a, b) Processing of the powders; c, d) photographs and SEM images of the pellets before and after temperature dependent measurements of electrical conductivity and Seebeck coefficient; e, f) electrical conductivity and Seebeck coefficient of the pellets measured 3 consecutive heating and cooling cycles from room temperature to 540 °C.



The difficulty to reduce these oxides is reflected in the high Gibbs free energies (Equation 4). Studies on H_2 gas adsorption on SnO indicate that annealing at 200 °C cannot remove SnO completely.^[76] In the treatment reported by Lee et al. the SnSe powder was annealed at 340 °C for 6 h (4 % H_2 in Ar),^[42] which effectively reduced the amount of SnO_2 present. Shorter time can be used at higher temperatures. Here, we compared the samples annealed with inert gas and with a reducing atmosphere.

We prepared SnSe pellets with powders annealed under inert atmosphere (N_2 , 0.3 L min^{-1} , 500 °C for 1 h) and under forming gas (5 % H_2 in N_2 , 0.3 L min^{-1} , 500 °C for 1 h), and characterized their structural and transport properties (Figure 6). SEM of the annealed powders (Figure 6a) reveals that in both cases annealing leads to an increase in the grain size, although the effect is enhanced by forming gas. This effect is even more prominent after densification of the

annealed powders. We attribute the difference in grain sizes to the presence of SnO_2 in the samples, confirmed by XRD (SnO_2 ; $2\theta = 34^\circ$ reflection, Figure 6d, Figure S16). SnO_2 is not miscible with SnSe and forms second phase particles that pin the grain boundaries (Zener pinning) inhibiting grain growth^[74] (Figure S16) and could also act as a diffusion barrier for Sn^{2+} and Se^{2-} , retarding sintering and coarsening.^[77,78]

The reduction of oxides during the particle annealing and the larger grain size have a noticeable impact on the charge transport properties (Figure 6e–h). The sample treated in a reducing atmosphere has higher charge carrier mobility and σ than the sample annealed under inert gas flow (Figure 6h). This results from the reduced density of grain boundaries and secondary phase oxides, thereby decreasing charge carrier scattering. A similar effect is observed for the κ_{lattice} , which is higher in the low temperature range due to the decrease in grain boundary phonon scattering for the sample treated with forming gas (Figure 6g). Interestingly, the κ_{lattice} does not decrease with the removal of oxides, consistent with the recent findings.^[50]

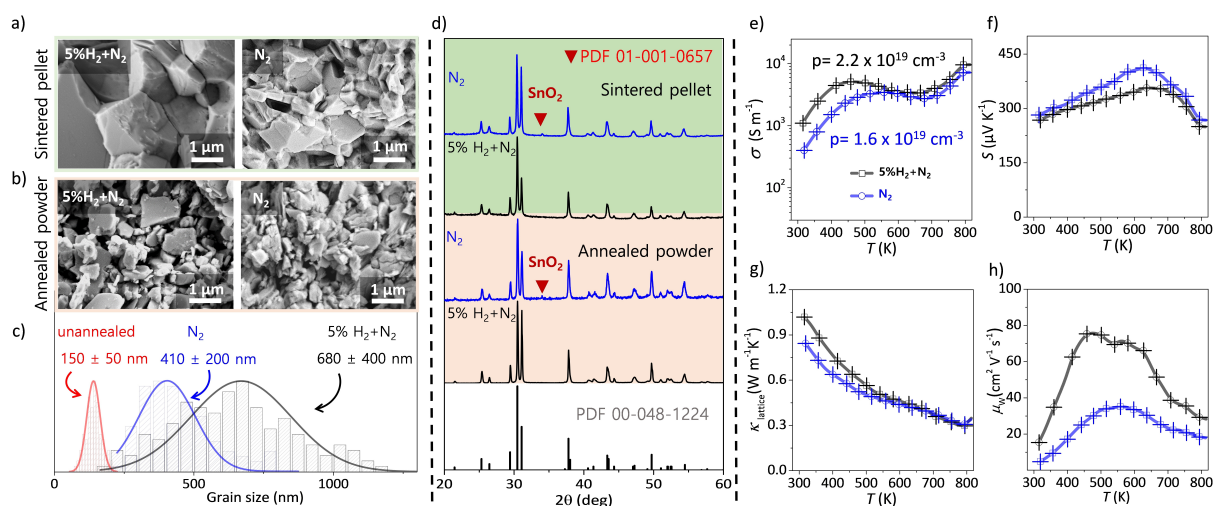


Figure 6. The effect of annealing atmosphere on the structure and properties of SnSe. SEM images of a) sintered pellets under inert and reducing atmospheres and b) annealed powders. c) size distribution of unannealed and annealed powder under inert and reducing atmosphere, d) XRD patterns of the SnSe powders annealed under inert and reducing atmospheres and corresponding pellets, indicating the presence of SnO₂ (PDF 01-001-0657), e–h) transport properties of these samples.

To interpret this apparent contradiction with the reported role of annealing treatments to reduce the thermal conductivity,^[26] it is important to note that, in comparison with samples prepared by ball milling, samples prepared in solution have a much larger content of oxides.^[42] Therefore, a short reductive treatment with low temperatures cannot completely remove the oxides, and the change in thermal conductivity is dominated by the difference in grain size. However, if longer annealing treatments are performed or if the annealing temperature is increased, the thermal conductivity is effectively reduced. (Figure S17; annealing temperature). The effect of sintering conditions on the materials' microstructure and transport properties were also evaluated. The samples showed no major variations when the temperature was changed to consolidate the bulk materials (Figure S18).

3. Conclusions

In this work, we explored the chemistry involved in the purification process of solution-processed TE materials with a focus on aqueous-based SnSe. We show that the solvent choice, number of leaching steps, annealing and choice of annealing atmosphere play a critical role in influencing the composition, microstructure evolution and transport properties of the final material. More specifically we highlight that: i) water is more efficient in removing Sn and ethanol is more efficient in removing Se, as solvents used in the leaching process ii) at $\times 6$ leaching steps there is optimal power factor due to the tradeoff between the σ and S , iii) annealing improves mechanical stability, by promoting grain growth and removing any volatile or labile species and iv) a reducing atmosphere aids in the reduction of oxides in the consolidated material. Overall, this work illustrates the

relevance of understanding the chemistry of each processing parameter in the solution-processing of materials to rationally optimize material performance. Additionally, we aim to highlight the importance of following a systematic approach, thoroughly understanding each procedural step through detailed characterization, and meticulously documenting all aspects of the processing procedure so no crucial information with overlooked value is left out of experimental procedures, hence ensuring the reproducibility of the results reported.

4. Supporting Information

The authors have cited additional references within the Supporting Information.^[80–99]

Acknowledgements

ISTA and the Werner Siemens Foundation financially supported this work. The Scientific Service Units (SSU) of ISTA supported this research through resources provided by the Electron Microscopy Facility (EMF), NMR Facility and the Lab Support Facility (LSF). Dr. Krishnendu Maji at ISTA aided in this work through XRD analysis of the crystal phase of SnSe. Y.L. acknowledges funding from the European Union's Horizon 2020 research and innovation program under the Marie Skłodowska-Curie grant agreement No. 754411, the National Natural Science Foundation of China (NSFC) (Grants No. 22209034). M.C. received funding from the European Union's Horizon 2020 research and innovation program under the Marie Skłodowska-Curie Grant Agreement No. 665385.

Conflict of Interest

The authors declare no conflict of interest.

Data Availability Statement

The data that support the findings of this study are available from the corresponding author upon reasonable request.

Keywords: grain coarsening · nanoparticles · purification · solution-processed · thermoelectrics

- [1] X.-L. Shi, J. Zou, Z.-G. Chen, *Chem. Rev.* **2020**, *120*, 7399–7515.
- [2] B. Ryu, J. Chung, M. Kumagai, T. Mato, Y. Ando, S. Gunji, A. Tanaka, D. Yana, M. Fujimoto, Y. Imai, Y. Katsura, S. Park, *iScience* **2023**, *26*, 106494.
- [3] J. Orton, in *The Story of Semiconductors* (Ed.: J. W. Orton), Oxford University Press **2008**, p. 0.
- [4] A. Zevalkink, D. M. Smiadak, J. L. Blackburn, A. J. Ferguson, M. L. Chabiny, O. Delaire, J. Wang, K. Kovnir, J. Martin, L. T. Schelhas, T. D. Sparks, S. D. Kang, M. T. Dylla, G. J. Snyder, B. R. Ortiz, E. S. Toberer, *Appl. Phys. Rev.* **2018**, *5*, 021303.
- [5] X.-L. Shi, W.-D. Liu, M. Li, Q. Sun, S.-D. Xu, D. Du, J. Zou, Z.-G. Chen, *Adv. Energy Mater.* **2022**, *12*, 2200670.
- [6] N. Nandihalli, D. H. Gregory, T. Mori, *Adv. Sci.* **2022**, *9*, 2106052.
- [7] M. Li, Y. Liu, Y. Zhang, C. Chang, T. Zhang, D. Yang, K. Xiao, J. Arbiol, M. Ibáñez, A. Cabot, *Chem. Eng. J.* **2022**, *433*, 133837.
- [8] S. Y. Tee, X. Y. Tan, X. Wang, C. J. J. Lee, K. Y. Win, X. P. Ni, S. L. Teo, D. H. L. Seng, Y. Tanaka, M.-Y. Han, *Inorg. Chem.* **2022**, *61*, 6451–6458.
- [9] T. Kleinhanns, F. Milillo, M. Calcabrini, C. Fiedler, S. Horta, D. Balazs, M. J. Strumolo, R. Hasler, J. Llorca, M. Tkadletz, R. L. Brutchey, M. Ibáñez, *Adv. Energy Mater.* n.d., *n/a*, 2400408.
- [10] S. Ortega, M. Ibáñez, Y. Liu, Y. Zhang, M. V. Kovalenko, D. Cadavid, A. Cabot, *Chem. Soc. Rev.* **2017**, *46*, 3510–3528.
- [11] S. Chandra, K. Biswas, *J. Am. Chem. Soc.* **2019**, *141*, 6141–6145.
- [12] M. Ibáñez, R. Zamani, W. Li, D. Cadavid, S. Gorsse, N. A. Katcho, A. Shavel, A. M. López, J. R. Morante, J. Arbiol, A. Cabot, *Chem. Mater.* **2012**, *24*, 4615–4622.
- [13] Z. Hens, J. De Roo, *J. Am. Chem. Soc.* **2020**, *142*, 15627–15637.
- [14] C. Fiedler, T. Kleinhanns, M. Garcia, S. Lee, M. Calcabrini, M. Ibáñez, *Chem. Mater.* **2022**, *34*, 8471–8489.
- [15] Y. Liu, M. Calcabrini, Y. Yu, S. Lee, C. Chang, J. David, T. Ghosh, M. C. Spadaro, C. Xie, O. Cojocar-Mirédin, J. Arbiol, M. Ibáñez, *ACS Nano* **2022**, *16*, 78–88.
- [16] C. Chang, M. Ibáñez, *Materials* **2021**, *14*, 5416.
- [17] Y. Liu, M. Li, S. Wan, K. H. Lim, Y. Zhang, M. Li, J. Li, M. Ibáñez, M. Hong, A. Cabot, *ACS Nano* **2023**, *17*, 11923–11934.
- [18] A. Heuer-Jungemann, N. Feliu, I. Bakaimi, M. Hamaly, A. Alkilany, I. Chakraborty, A. Masood, M. F. Casula, A. Kostopoulou, E. Oh, K. Susumu, M. H. Stewart, I. L. Medintz, E. Stratakis, W. J. Parak, A. G. Kanaras, *Chem. Rev.* **2019**, *119*, 4819–4880.
- [19] X. Li, C. Chen, W. Xue, S. Li, F. Cao, Y. Chen, J. He, J. Sui, X. Liu, Y. Wang, Q. Zhang, *Inorg. Chem.* **2018**, *57*, 13800–13808.
- [20] D. Ding, C. Lu, Z. Tang, *Adv. Mater. Interfaces* **2017**, *4*, 1700517.
- [21] X. Lou, S. Li, X. Chen, Q. Zhang, H. Deng, J. Zhang, D. Li, X. Zhang, Y. Zhang, H. Zeng, G. Tang, *ACS Nano* **2021**, *15*, 8204–8215.
- [22] J. Liu, P. Wang, M. Wang, R. Xu, J. Zhang, J. Liu, D. Li, N. Liang, Y. Du, G. Chen, G. Tang, *Nano Energy* **2018**, *53*, 683–689.
- [23] R. Xu, L. Huang, J. Zhang, D. Li, J. Liu, J. Liu, J. Fang, M. Wang, G. Tang, *J. Mater. Chem. A* **2019**, *7*, 15757–15765.
- [24] S. Li, X. Lou, X. Li, J. Zhang, D. Li, H. Deng, J. Liu, G. Tang, *Chem. Mater.* **2020**, *32*, 9761–9770.
- [25] M. Li, Y. Liu, Y. Zhang, Y. Zuo, J. Li, K. H. Lim, D. Cadavid, K. M. Ng, A. Cabot, *Dalton Trans.* **2019**, *48*, 3641–3647.
- [26] C. Zhou, Y. K. Lee, Y. Yu, S. Byun, Z.-Z. Luo, H. Lee, B. Ge, Y.-L. Lee, X. Chen, J. Y. Lee, O. Cojocar-Mirédin, H. Chang, J. Im, S.-P. Cho, M. Wuttig, V. P. Dravid, M. G. Kanatzidis, I. Chung, *Nat. Mater.* **2021**, *20*, 1378–1384.
- [27] A. C. Arias, J. D. MacKenzie, I. McCulloch, J. Rivnay, A. Salleo, *Chem. Rev.* **2010**, *110*, 3–24.
- [28] Z.-H. Ge, K. Wei, H. Lewis, J. Martin, G. S. Nolas, *J. Solid State Chem.* **2015**, *225*, 354–358.
- [29] L. De Trizio, L. Manna, *Chem. Rev.* **2016**, *116*, 10852–10887.
- [30] D. D. I. Vaughn, S.-I. In, R. E. Schaak, *ACS Nano* **2011**, *5*, 8852–8860.
- [31] G. Han, S. R. Popuri, H. F. Greer, J.-W. G. Bos, W. Zhou, A. R. Knox, A. Montecucco, J. Siviter, E. A. Man, M. Macauley, D. J. Paul, W. Li, M. C. Paul, M. Gao, T. Sweet, R. Freer, F. Azough, H. Baig, N. Sellami, T. K. Mallick, D. H. Gregory, *Angew. Chem. Int. Ed.* **2016**, *55*, 6433–6437.
- [32] C. L. McCarthy, R. L. Brutchey, *Chem. Commun.* **2017**, *53*, 4888–4902.
- [33] D. H. Webber, R. L. Brutchey, *J. Am. Chem. Soc.* **2013**, *135*, 15722–15725.
- [34] H. S. Wasly, M. S. A. El-Sadek, M. Henini, *Appl. Phys. A* **2018**, *124*, 76.
- [35] X.-L. Shi, X. Tao, J. Zou, Z.-G. Chen, *Adv. Sci.* **2020**, *7*, 1902923.
- [36] L. Das, A. Guleria, S. Adhikari, *RSC Adv.* **2015**, *5*, 61390–61397.
- [37] M. Ibáñez, D. Cadavid, U. Anselmi-Tamburini, R. Zamani, S. Gorsse, W. Li, A. M. López, J. R. Morante, J. Arbiol, A. Cabot, *J. Mater. Chem. A* **2013**, *1*, 1421–1426.
- [38] J. Pei, G. Chen, X. Li, Y. X. Li, N. Zhou, *Mater. Lett.* **2009**, *63*, 1459–1461.
- [39] H. Wang, X. Liu, B. Zhang, L. Huang, M. Yang, X. Zhang, H. Zhang, G. Wang, X. Zhou, G. Han, *Chem. Eng. J.* **2020**, *393*, 124763.
- [40] Y. Min, J. W. Roh, H. Yang, M. Park, S. I. Kim, S. Hwang, S. M. Lee, K. H. Lee, U. Jeong, *Adv. Mater.* **2013**, *25*, 1425–1429.
- [41] G. Han, S. R. Popuri, H. F. Greer, L. F. Llin, J. G. Bos, W. Zhou, D. J. Paul, H. Ménard, A. R. Knox, A. Montecucco, J. Siviter, E. A. Man, W. Li, M. C. Paul, M. Gao, T. Sweet, R. Freer, F. Azough, H. Baig, T. K. Mallick, D. H. Gregory, *Adv. Energy Mater.* **2017**, *7*, 1602328.
- [42] Y. K. Lee, Z. Luo, S. P. Cho, M. G. Kanatzidis, I. Chung, *Joule* **2019**, *3*, 719–731.
- [43] Y. Liu, M. Calcabrini, Y. Yu, A. Genç, C. Chang, T. Costanzo, T. Kleinhanns, S. Lee, J. Llorca, O. Cojocar-Mirédin, M. Ibáñez, Y. Liu, M. Calcabrini, C. Chang, T. Costanzo, T. Kleinhanns, S. Lee, M. Ibáñez, Y. Yu, O. Cojocar-Mirédin, R. Aachen, A. Genç, *Adv. Mater.* **2021**, 2106858.
- [44] S. Chakraborty, S. K. Misra, *Environ. Nanotechnol., Monit. Manage.* **2019**, *12*, 100258.
- [45] J. D. Robertson, L. Rizzello, M. Avila-Olias, J. Gaitzsch, C. Contini, M. S. Magoñ, S. A. Renshaw, G. Battaglia, *Sci. Rep.* **2016**, *6*, 27494.

- [46] G.-T. Wei, F.-K. Liu, C. R. C. Wang, *Anal. Chem.* **1999**, *71*, 2085–2091.
- [47] V. Sharma, K. Park, M. Srinivasarao, *Proc. Natl. Acad. Sci. USA* **2009**, *106*, 4981–4985.
- [48] X. Xu, H. Cölfen, *Nanomaterials (Basel)* **2021**, *11*, 333.
- [49] Z.-H. Ge, D. Song, X. Chong, F. Zheng, L. Jin, X. Qian, L. Zheng, R. E. Dunin-Borkowski, P. Qin, J. Feng, L.-D. Zhao, *J. Am. Chem. Soc.* **2017**, *139*, 9714–9720.
- [50] E. Isotta, M. Y. Toriyama, A. H. Adekoya, R. Shupp, G. J. Snyder, A. Zevalkink, *Mater. Today Phys.* **2023**, *31*, 100967.
- [51] V. Q. Nguyen, T. L. Trinh, C. Chang, L.-D. Zhao, T. H. Nguyen, V. T. Duong, A. T. Duong, J. H. Park, S. Park, J. Kim, S. Cho, *NPG Asia Mater.* **2022**, *14*, 1–7.
- [52] Y. Huang, C. Wang, X. Chen, D. Zhou, J. Du, S. Wang, L. Ning, *RSC Adv.* **2017**, *7*, 27612–27618.
- [53] L.-D. Zhao, S.-H. Lo, Y. Zhang, H. Sun, G. Tan, C. Uher, C. Wolverton, V. P. Dravid, M. G. Kanatzidis, *Nature* **2014**, *508*, 373–377.
- [54] S. Bhanushali, P. Ghosh, A. Ganesh, W. Cheng, *Small* **2015**, *11*, 1232–1252.
- [55] Y.-X. Chen, Z.-H. Ge, M. Yin, D. Feng, X.-Q. Huang, W. Zhao, J. He, *Adv. Funct. Mater.* **2016**, *26*, 6836–6845.
- [56] D. Feng, Z.-H. Ge, D. Wu, Y.-X. Chen, T. Wu, J. Li, J. He, *Phys. Chem. Chem. Phys.* **2016**, *18*, 31821–31827.
- [57] E. Nes, N. Ryum, O. Hunderi, *Acta Metall.* **1985**, *33*, 11–22.
- [58] L. D. Zhao, B.-P. Zhang, J.-F. Li, H. L. Zhang, W. S. Liu, *Solid State Sci.* **2008**, *10*, 651–658.
- [59] J. Jiang, L. Chen, S. Bai, Q. Yao, Q. Wang, *Mater. Sci. Eng. B* **2005**, *117*, 334–338.
- [60] K. Park, J. S. Son, S. I. Woo, K. Shin, M.-W. Oh, S.-D. Park, T. Hyeon, *J. Mater. Chem. A* **2014**, *2*, 4217–4224.
- [61] M. Ibáñez, D. Cadavid, R. Zamani, N. García-Castelló, V. Izquierdo-Roca, W. Li, A. Fairbrother, J. D. Prades, A. Shavel, J. Arbiol, A. Pérez-Rodríguez, J. R. Morante, A. Cabot, *Chem. Mater.* **2012**, *24*, 562–570.
- [62] M. Ibáñez, Z. Luo, A. Genç, L. Piveteau, S. Ortega, D. Cadavid, O. Dobrozhan, Y. Liu, M. Nachtgeal, M. Zabarjadi, J. Arbiol, M. V. Kovalenko, A. Cabot, *Nat. Commun.* **2016**, *7*, 10766.
- [63] C. Han, Z. Li, G. Q. (Max) Lu, S. Xue Dou, *Nano Energy* **2015**, *15*, 193–204.
- [64] M. Ibáñez, A. Genç, R. Hasler, Y. Liu, O. Dobrozhan, O. Nazarenko, M. de la Mata, J. Arbiol, A. Cabot, M. V. Kovalenko, *ACS Nano* **2019**, *13*, 6572–6580.
- [65] A. Nag, M. V. Kovalenko, J.-S. Lee, W. Liu, B. Spokoyny, D. V. Talapin, *J. Am. Chem. Soc.* **2011**, *133*, 10612–10620.
- [66] T.-R. Wei, G. Tan, X. Zhang, C.-F. Wu, J.-F. Li, V. P. Dravid, G. J. Snyder, M. G. Kanatzidis, *J. Am. Chem. Soc.* **2016**, *138*, 8875–8882.
- [67] M. Johnson, S. V. Baryshev, E. Thimsen, M. Manno, X. Zhang, I. V. Veryovkin, C. Leighton, E. S. Aydil, *Energy Environ. Sci.* **2014**, *7*, 1931–1938.
- [68] J. Sangster, A. D. Pelton, *JPE* **1997**, *18*, 185–189.
- [69] V. Riesgo-González, D. S. Hall, K. Märker, J. Slaughter, D. S. Wright, C. P. Grey, *Chem. Mater.* **2022**, *34*, 9722–9735.
- [70] N. Tsuboi, Y. Itoh, J. Ogata, S. Kobayashi, H. Shimizu, K. Kato, F. Kaneko, *jjap* **2007**, *46*, 351.
- [71] M. Mattinen, P. J. King, L. Khriachtchev, M. J. Heikkilä, B. Fleming, S. Rushworth, K. Mizohata, K. Meinander, J. Räisänen, M. Ritala, M. Leskelä, *Mater. Today Chem.* **2018**, *9*, 17–27.
- [72] M. M. Hessien, M. M. Rashad, K. El-Barawy, *J. Magn. Magn. Mater.* **2008**, *320*, 336–343.
- [73] M. Li, Y. Liu, Y. Zhang, X. Han, T. Zhang, Y. Zuo, C. Xie, K. Xiao, J. Arbiol, J. Llorca, M. Ibáñez, J. Liu, A. Cabot, *ACS Nano* **2021**, *15*, 4967–4978.
- [74] Y. Li, B. He, J. P. Heremans, J. C. Zhao, *J. Alloys Compd.* **2016**, *669*, 224–231.
- [75] L. D. Zhao, C. Chang, G. Tan, M. G. Kanatzidis, *Energy Environ. Sci.* **2016**, *9*, 3044–3060.
- [76] D. O. Scanlon, G. W. Watson, *J. Mater. Chem.* **2012**, *22*, 25236–25245.
- [77] A. R. Hingorany, F. V. Lenel, G. S. Ansell, in *Kinetics of Reactions in Ionic Systems* (Eds.: T. J. Gray, V. D. Fréchet), Springer US, Boston, MA **1969**, pp. 375–391.
- [78] S.-J. L. Kang, Y.-I. Jung, *Acta Mater.* **2004**, *52*, 4573–4578.
- [79] G. Han, S. R. Popuri, H. F. Greer, R. Zhang, L. Ferre-Llin, J.-W. G. Bos, W. Zhou, M. J. Reece, D. J. Paul, A. R. Knox, D. H. Gregory, *Chem. Sci.* **2018**, *9*, 3828–3836.
- [80] É. G. Bajnóczi, E. Czeplédi, E. Kuzmann, Z. Homonnay, S. Bálint, G. Dombi, P. Forgo, O. Berkesi, I. Pálkó, G. Peintler, P. Sipos, I. Persson, *Dalton Trans.* **2014**, *43*, 17971–17979.
- [81] J. Schott, J. Kretschmar, M. Acker, S. Eidner, M. U. Kumke, B. Drobot, S. Taut, A. Barkleit, T. Stumpf, *Dalton Trans.* **2014**, *43*, 11516–11528.
- [82] D. E. Levy, R. J. Myers, *J. Phys. Chem.* **1990**, *94*, 7842–7847.
- [83] S. Licht, F. Forouzan, *J. Electrochem. Soc.* **1995**, *142*, DOI 10.1149/1.2048610.
- [84] W. M. Haynes, Ed., *CRC Handbook of Chemistry and Physics*, CRC Press, Boca Raton **2016**.
- [85] S. Boone, O. J. Kleppa, *Thermochim. Acta* **1992**, *197*, 109–121.
- [86] H. Wiedemeier, G. Pultz, U. Gaur, B. Wunderlich, *Thermochim. Acta* **1981**, *43*, 297–303.
- [87] “Chemical Thermodynamics of Tin, Volume 12|en|OECD,” can be found under <https://www.oecd.org/publications/chemical-thermodynamics-of-tin-volume-12-9789264992061-en.htm>, n.d.
- [88] N. A. Lange, *Lange’s Handbook of Chemistry*, McGraw-Hill, New York, NY **1999**.
- [89] P. Atkins, *Shriver and Atkins’ Inorganic Chemistry*, OUP Oxford **2010**.
- [90] L. E. Lyons, T. L. Young, *Aust. J. Chem.* **1986**, *39*, 511–527.
- [91] A. Goldbach, M.-L. Saboungi, J. A. Johnson, A. R. Cook, D. Meisel, *J. Phys. Chem. A* **2000**, *104*, 4011–4016.
- [92] B. Pejjai, V. R. Minnam Reddy, K. Seku, M. R. Pallavolu, C. Park, *New J. Chem.* **2018**, *42*, 4843–4853.
- [93] J. M. Lalancette, M. Arnac, *Can. J. Chem.* **1969**, *47*, 3695–3697.
- [94] M. Yarema, O. Yarema, W. M. M. Lin, S. Volk, N. Yazdani, D. Bozyigit, V. Wood, *Chem. Mater.* **2017**, *29*, 796–803.
- [95] S. Li, Y. Hou, S. Zhang, Y. Gong, S. Siddique, D. Li, J. Fang, P. Nan, B. Ge, G. Tang, *Chem. Eng. J.* **2023**, *451*, 138637.
- [96] X. Shi, K. Zheng, M. Hong, W. Liu, R. Moshwan, Y. Wang, X. Qu, Z.-G. Chen, J. Zou, *Chem. Sci.* **2018**, *9*, 7376–7389.
- [97] R. M. Cigala, F. Crea, C. De Stefano, G. Lando, D. Milea, S. Sammartano, *Geochim. Cosmochim. Acta* **2012**, *87*, 1–20.
- [98] G. Shi, E. Kioupakis, *J. Appl. Phys.* **2015**, *117*, 065103.
- [99] A. B. Garrett, R. E. Heiks, *J. Am. Chem. Soc.* **1941**, *63*, 562–567.

Manuscript received: February 5, 2024

Accepted manuscript online: April 16, 2024

Version of record online: May 16, 2024